ELSEVIER

Applied Numerical Mathematics 32 (2000) 1–20

APPLIED NUMERICAL MATHEMATICS

www.elsevier.nl/locate/apnum

The effect of quadrature on the dynamics of a discretized nonlinear integro-differential equation

Mark A. Aves [a,1,3], Penny J. Davies [b,2], Desmond J. Higham [b,*,3]

[a] *Concept Systems, 1 Logie Mill, Beaverbank Business Park, Logie Green Road, Edinburgh EH7 4HG, UK*

[b] *Department of Mathematics, University of Strathclyde, 26 Richmond St., Glasgow G1 1XH, UK*

Abstract

The long-term dynamics of a discretized, nonlinear, integro-differential equation with convolution kernel are studied. For a constant time-step algorithm the existence and stability of fixed and periodic points are investigated. A systematic treatment is given, which quantifies the effect of varying the quadrature rule and integrating the kernel exactly or approximately. Special attention is paid to spurious behaviour that occurs below, or around, the "natural" time-step that corresponds to the linear stability limit for the correct fixed point. It is shown that spurious solutions exist, and can be computed, within this linear stability range. In addition to fixed points and period two solutions, analysis is performed for a class of period three orbits that are observed to be relevant to the long-term dynamics. Finally, an adaptive algorithm, based on local error control, is studied and a simple model describing its long-term behaviour is developed.

Keywords: Convolution kernel; Error control; Period two; Long-term dynamics; Linear stability; Spurious solution; Time-stepping

1. Introduction

A variety of mathematical models are used in the study of population dynamics. One model that has been proposed [3,12,13] is an integro-differential equation (IDE), which in its non-dimensionalized form can be written as

$$\phi'(t) = \phi(t)\left(1 - \int_{-\infty}^{t} K(t-\tau)\,\phi(\tau)\,d\tau\right) \quad \text{for } t > 0, \tag{1.1}$$

* Corresponding author. E-mail: d.j.higham@strath.ac.uk

[1] E-mail: maves@csl.co.uk

[2] These authors acknowledge funding by the UK EPSRC under research grant number GR/K80228.

[3] E-mail: penny.davies@strath.ac.uk

0168-9274/00/$20.00
PII: S0168-9274(99)00013-6

where $\phi(t)$ is given for $t \leqslant 0$ and the kernel $K(t)$ satisfies

$$\int_0^\infty K(s)\,\mathrm{d}s = 1.$$

Our aim in this work is to study the behaviour of a class of numerical methods for problems of the form (1.1). We are particularly concerned with the way in which the long-term behaviour of the numerical solution depends on the stepsize, and on the type of quadrature approximations used. Some initial analysis was performed in [1] for the kernel

$$K(t) = \frac{t\,\mathrm{e}^{-t/T}}{T^2}. \tag{1.2}$$

Here we consider the alternative kernel

$$K(t) = \frac{\mathrm{e}^{-t/T}}{T}. \tag{1.3}$$

Both (1.2) and (1.3) have been used in population models [3,12,13], with the constant $T > 0$ regarded as a delay parameter. The kernel (1.3) is easier to deal with than (1.2), and hence in this work we are able to extend the type of analysis that appears in [1]. In particular, we analyze stability of periodic solutions and also look at the impact of error control.

The IDE (1.1) has fixed points $\phi(t) \equiv \{0, 1\}$, whose linear stability can been studied via the Laplace transform [3,12]. It is straightforward to check that the zero fixed point is linearly unstable, and to investigate the stability of the non-zero fixed point we set $\phi(t) = 1 + \varepsilon(t)$ and linearize to obtain

$$\varepsilon'(t) = -\int_0^t K(t-\tau)\varepsilon(\tau)\,\mathrm{d}\tau + \gamma(t),$$

where

$$\gamma(t) = -\int_0^\infty K(t+\tau)\,\varepsilon(-\tau)\,\mathrm{d}\tau$$

involves the perturbation of the initial data. Stability of this linear convolution problem is equivalent to the condition

$$z + \widehat{K}(z) \neq 0 \quad \text{for all } z \in \mathbb{C} \text{ with } \Re\{z\} \geqslant 0, \tag{1.4}$$

where $\widehat{K}(z)$ is the Laplace transform

$$\widehat{K}(z) = \int_0^\infty K(s)\,\mathrm{e}^{-zs}\,\mathrm{d}s.$$

For the kernel (1.3) condition (1.4) is equivalent to $P(z) \neq 0$ whenever $\Re\{z\} \geqslant 0$, where $P(z) = Tz^2 + z + 1$. This is satisfied for all $T > 0$. (If $0 < T \leqslant \frac{1}{4}$ then P has two negative real roots, and P has complex conjugate roots with negative real part for $T > \frac{1}{4}$.) Hence the fixed point $\phi(t) \equiv 1$ of the IDE (1.1) with kernel (1.3) is linearly stable for all $T > 0$. In this work we are concerned with the existence and stability of the analogous non-zero steady state and other long-term solutions of discretizations of this IDE.

2. The discretization

We discretize the IDE (1.1) using Euler's method with time-step h to approximate the time derivative and a quadrature rule for the integral. The Euler approximation gives

$$\Phi_{n+1} = \Phi_n + h\Phi_n\left(1 - \sum_{j=0}^{\infty} \int_{(n-j-1)h}^{(n-j)h} K(nh-s)\,\Phi(s)\,\mathrm{d}s\right), \tag{2.1}$$

where $\Phi(s) \approx \phi(s)$, $\Phi_m = \Phi(mh)$ and we have used the integral identity

$$\int_{-\infty}^{nh} K(nh-\tau)\,\Phi(\tau)\,\mathrm{d}\tau = \sum_{j=0}^{\infty} \int_{(n-j-1)h}^{(n-j)h} K(nh-s)\Phi(s)\,\mathrm{d}s.$$

Applying a simple quadrature rule to approximate the convolution integral in (2.1) leads to a recurrence of the form

$$\Phi_{n+1} = \Phi_n + h\Phi_n\left(1 - \sum_{j=0}^{\infty} \omega_j\,\Phi_{n-j}\right). \tag{2.2}$$

Here, the weights ω_j are determined by the choice of quadrature rule. We consider quadrature rules that are found by assuming either a piecewise constant (PC) or a piecewise linear (PL) variation of the solution Φ over a time-step. This produces the infinite discrete map

$$\Phi_{n+1} = \Phi_n + h\Phi_n\left(1 - \sum_{j=0}^{\infty} \Phi_{n-j}\,W_j\right) \tag{2.3}$$

for the PC case and

$$\Phi_{n+1} = \Phi_n + h\Phi_n\left(1 - \sum_{j=0}^{\infty} \left[(j+1)W_j - V_j\right]\Phi_{n-j} + \left[V_j - jW_j\right]\Phi_{n-j-1}\right) \tag{2.4}$$

for the PL case. The terms W_j and V_j are found by either exact or approximate integration of the kernel:

$$W_j \approx \int_{jh}^{(j+1)h} K(s)\,\mathrm{d}s, \qquad V_j \approx \frac{1}{h}\int_{jh}^{(j+1)h} s\,K(s)\,\mathrm{d}s. \tag{2.5}$$

The kernel (1.3) is sufficiently simple to allow the integrals in (2.5) to be evaluated exactly. However, for more complicated kernels a quadrature formula must be used. In our study, we consider exact integration in (2.5) and also the case where the kernel is approximated by a piecewise constant or piecewise linear function on each time-step. The relevant weights are

$$\text{PC approximation:} \quad W_j = rq^j, \qquad V_j = \left(j+\tfrac{1}{2}\right)W_j, \tag{2.6}$$

$$\text{PL approximation:} \quad W_j = \frac{r}{2}\left(q^j + q^{j+1}\right), \qquad V_j = \frac{r}{6}\left((3j+1)q^j + (3j+2)q^{j+1}\right), \tag{2.7}$$

$$\text{exact evaluation:} \quad W_j = q^j - q^{j+1}, \qquad V_j = (j+1/r)q^j - (j+1+1/r)q^{j+1}, \tag{2.8}$$

where $r = h/T$ and $q = \mathrm{e}^{-r}$.

This results in six different approximations of the IDE (1.1) by independently choosing between the two maps (2.3) and (2.4) and the three different ways of evaluating the weights (PC, PL or exact integration). We label each of these approximations by a pair of letters from the set {C, L, E} (denoting PC and PL quadrature and exact integration), with the first letter representing the type of approximation used for the solution Φ (i.e., C or L) and the second the way of calculating the weights (2.5) (i.e., C, L or E). Thus the different possibilities can be denoted by the set {CC, CL, CE, LC, LL, LE}, where, e.g., CL means that the approximation uses the map (2.3) with the kernel weights W_j approximated by piecewise linear functions and given by (2.7).

3. Fixed points of the discrete maps

The fixed points or steady states of the map (2.2) are found by setting the solution Φ_j to be a constant for all j. The map has two fixed points, $\Phi_j \in \{0, \Phi^*\}$, where

$$\Phi^* = \left(\sum_{j=0}^{\infty} \omega_j \right)^{-1}. \tag{3.1}$$

For both the PC and PL solution approximations the non-zero fixed point (3.1) is given by

$$\Phi^* = \left(\sum_{j=0}^{\infty} W_j \right)^{-1}.$$

Substituting the weight formulae (2.6)–(2.8) into Eq. (3.1) then gives the non-zero fixed point of the infinite discrete map (2.2) as

$$\Phi^* = \begin{cases} (1-q)/r & \text{for CC and LC,} \\ \dfrac{2(1-q)}{r(1+q)} & \text{for CL and LL,} \\ 1 & \text{for CE and LE,} \end{cases} \tag{3.2}$$

where recall that $r = h/T$ and $q = \mathrm{e}^{-r}$. These are plotted against r in Fig. 1. Note that when the weights (2.5) are evaluated exactly then Φ^* is the true fixed point of the continuous equation (1.1), while $\Phi^* \to 1$ as $h \to 0$ for the approximate weights.

3.1. Stability of the fixed points

It is easy to show that the zero fixed point of (2.2) is linearly unstable for any choice of weights ω_j. We now examine the linear stability of the non-zero fixed point Φ^* of the infinite map (2.2) for each of the six choices of weights ω_j described in the previous section. To do this set $\Phi_n = \Phi^* + \varepsilon_n$ and linearize to obtain the perturbation equation

$$\varepsilon_{n+1} = \varepsilon_n - h\Phi^* \sum_{j=0}^{\infty} \omega_j \varepsilon_{n-j}. \tag{3.3}$$

As shown in [1], a theorem due to Lubich [11] can be used to investigate the stability of the fixed point. If the initial perturbations are bounded, i.e., if

$$|\varepsilon_n| \leqslant \varepsilon_{\max} < \infty \quad \text{for all } n \leqslant 0,$$

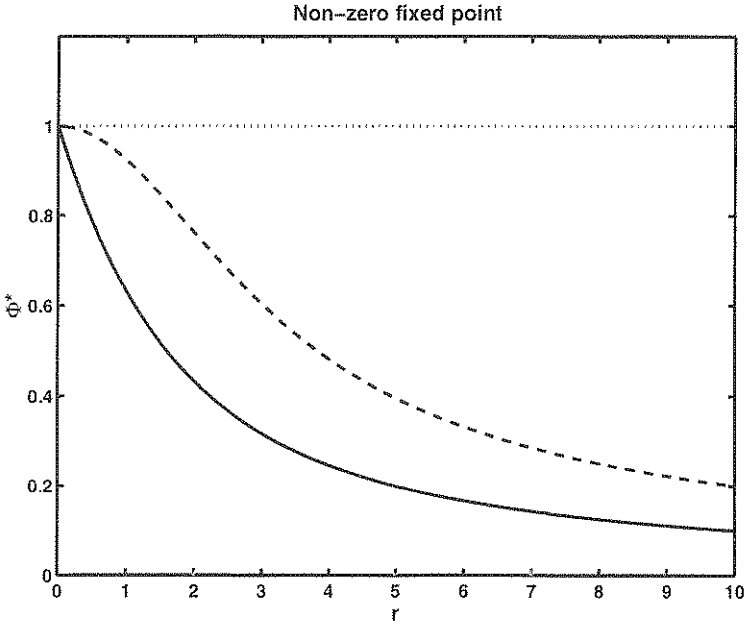

Fig. 1. Graphs of Φ^* against r for the maps CC & LC (solid), CL & LL (dashed), and CE & LE (dotted).

then Φ^* is linearly stable if and only if

$$1 - h\Phi^* \widehat{\omega}(z) \neq z \quad \text{for all } z \in \mathbb{C} \text{ with } |z| \geqslant 1. \tag{3.4}$$

Here, $\widehat{\omega}(z)$ denotes the Z-transform of the sequence $\{\omega_j\}$;

$$\widehat{\omega}(z) = \sum_{n=0}^{\infty} \omega_n z^{-n}.$$

The transform $\widehat{\omega}(z)$ is only defined for $|z| > 1/\rho$ where ρ is the radius of convergence of the power series $\sum_{j=0}^{\infty} \omega_j x^j$, and so for linear stability we only need to verify that if $|z| > 1/\rho$ and z solves (3.4) then $|z| < 1$. Note that this is equivalent to requiring any solution of (3.3) of the form $\varepsilon_j = z^j$ to satisfy $|z| < 1$. This technique can also be used to analyze the stability of the zero fixed point and reveals that it is unstable for all $h > 0$, irrespective of the way in which the solution weights are calculated.

We now examine (3.3) for each of the approximate maps derived in the previous subsection to find the maximum time-step h^* for which the corresponding fixed point Φ^* is linearly stable.

The stability equation (3.4) for the approximations CC, CL and CE reduces to

$$z^2 + z\left[h\left(1 - \mathrm{e}^{-r}\right) - \left(1 + \mathrm{e}^{-r}\right)\right] + \mathrm{e}^{-r} = 0. \tag{3.5}$$

For stability, we require that both roots satisfy $|z| < 1$, i.e., Eq. (3.5) is a Schur polynomial [10, pp. 13–14]. This is equivalent to the three inequalities below (which depend implicitly upon the delay through $r = h/T$)

$$0 < 2\left(1 + \mathrm{e}^{-r}\right) - h\left(1 - \mathrm{e}^{-r}\right), \tag{3.6}$$

$$0 < 2\left(1 - \mathrm{e}^{-r}\right), \tag{3.7}$$

$$0 < h\left(1 - \mathrm{e}^{-r}\right). \tag{3.8}$$

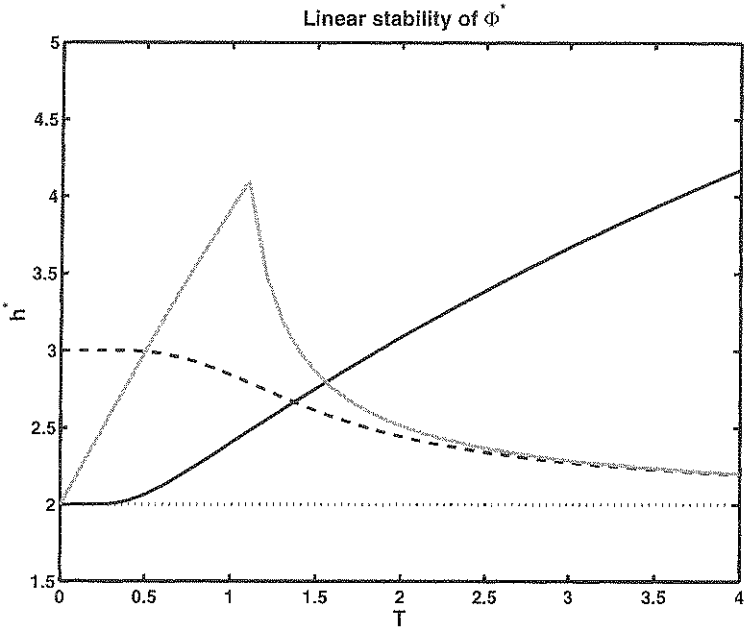

Fig. 2. Graphs to show the dependence of the time-step limit h^* on T for linear stability of the non-zero fixed point Φ^* for the CC, CL and CE maps (black solid), LC map (dotted), LL map (dashed) and LE map (grey solid).

Because $T > 0$, conditions (3.7) and (3.8) are satisfied for all $h > 0$. The limiting behaviour of (3.6) at equality for $T \gg 1$ and $T \ll 1$ gives $h^* \approx 2\sqrt{T}$ and $h^* \approx 2$, respectively. The stability bound can be easily computed for general values of T (e.g., if $T = 1$ then $h^* = 2 \cdot 399357281$) and is shown as the black solid line in Fig. 2.

The stability equation for the LC map is

$$2z^2 + z\left[h\left(1 - \mathrm{e}^{-r}\right) - 2\left(1 + \mathrm{e}^{-r}\right)\right] + h\left(1 - \mathrm{e}^{-r}\right) + 2\mathrm{e}^{-r} = 0. \tag{3.9}$$

The Schur conditions for this reduce to $h^* \equiv 2$ for all values of the delay, i.e., the fixed point is linearly stable for all $h \in (0, 2)$. This is shown as the dotted line in Fig. 2.

The situation in the LL case is more complicated. The stability equation is

$$\begin{aligned} &3\left(1 + \mathrm{e}^{-r}\right)z^2 + \left[h\left(2 + \mathrm{e}^{-r}\right)\left(1 - \mathrm{e}^{-r}\right) - 3\left(1 + \mathrm{e}^{-r}\right)^2\right]z \\ &\quad + h\left(1 + 2\mathrm{e}^{-r}\right)\left(1 - \mathrm{e}^{-r}\right) + 3\mathrm{e}^{-r}\left(1 + \mathrm{e}^{-r}\right) = 0, \end{aligned} \tag{3.10}$$

and the Schur conditions for stability when $h > 0$ are

$$h < 6\left(\frac{1 + \mathrm{e}^{-r}}{1 - \mathrm{e}^{-r}}\right)^2 \quad \text{and} \quad h < 3\left(\frac{1 + \mathrm{e}^{-r}}{1 + 2\mathrm{e}^{-r}}\right).$$

For h, $T > 0$, the second condition is always more restrictive and the stability boundary is shown as the dashed line in Fig. 2. The limiting cases $T \to 0$ and $T \to \infty$, give $h^* \to 3$ and $h^* \to 2$, respectively.

The stability equation for the LE case is

$$z^2 + z\left[h - 1 - \mathrm{e}^{-r} + T\left(\mathrm{e}^{-r} - 1\right)\right] + \mathrm{e}^{-r}(1 - h) + T\left(1 - \mathrm{e}^{-r}\right), \tag{3.11}$$

and this is Schur for all $h > 0$ satisfying the pair of inequalities

$$h < 2 + \frac{2T(1 - e^{-r})}{1 + e^{-r}} \quad \text{and} \quad h > (T - 1)(e^{r} - 1). \tag{3.12}$$

For $T \gg 1$ the second inequality is more restrictive and $h^* \to 2$ as $T \to \infty$. This inequality is satisfied for all $h > 0$ when $T < 1$ and so the stability limit is governed by the first inequality in this case, and $h^* \to 2$ from above as $T \to 0$. The inequalities cross at $T \approx 1 \cdot 10173$ and the stability bound is shown as the grey line in Fig. 2.

Overall, Fig. 2 summarizes the stability analysis from this section.

4. Numerical results

We now present some numerical results to illustrate the long-term behaviour of the map (2.2) with the particular weights ω_j derived in Section 2. In order to do this we approximate (2.2) by the finite map

$$\Phi_{n+1} = \Phi_n + h\Phi_n\left(1 - \sum_{j=0}^{N-1} \Phi_{n-j}\omega_j\right), \tag{4.1}$$

where N is a large, fixed number chosen to make the difference between the infinite and finite sums small. All the figures presented here were produced using $N = 100$; and this gives bifurcation plots that are visually identical to those produced using $N = 50$. The map (4.1) has the non-zero fixed point

$$\Phi_N^* = \left(\sum_{j=0}^{N-1} \omega_j\right)^{-1}.$$

Clearly, $\Phi_N^* \to \Phi^*$ as $N \to \infty$.

It is straightforward to show that for each map the weight functions ω_j for $j > 0$ all take the form $\omega_j = aq^j$ for some $a(r) > 0$, where a is independent of j, $a = \mathrm{O}(r)$ as $r \to 0$ and is an $\mathrm{O}(1)$ quantity when $r = \mathrm{O}(1)$. Hence the difference in the value of Φ_{n+1} computed from the infinite map (2.2) and truncated map (4.1) is bounded by

$$\frac{a(r)hc_n^2 q^N}{1 - q},$$

where $c_n = \max\{|\Phi_j|\colon\ j \leqslant n\}$. Therefore for any fixed h and T the difference can be made arbitrarily small by choosing N large enough. If $r = h/T$ is not too small then moderate values of N ensure that the finite and infinite maps are the same up to machine precision (provided the Φ_n stay bounded). For example, if $r = 0.5$ and $c_n = \mathrm{O}(1)$ then the difference between the finite and infinite maps can be made 10^{-16} by choosing $N \approx 80$.

The bifurcation diagrams shown in Figs. 3 and 4 are computed by iterating the map (4.1) 500 times for each value of $h \in [0.1 : 0.01 : 4]$ with constant initial data $\Phi_j = c_0$ for $j = 1 - N : 0$ for many different values of $c_0 \in [0, 2]$. The last 10 iterates $\{\Phi_j\}_{j=491}^{500}$ are plotted on the graph. As expected, the bifurcation diagrams reproduce the non-zero fixed point for $h < h^*$, where h^* is the linearized stability limit shown in Fig. 2. The fixed point of the CC, CL and CE maps appears to lose stability through period doubling, and each plot shows complicated dynamical behaviour for some values of h. In particular, note that there

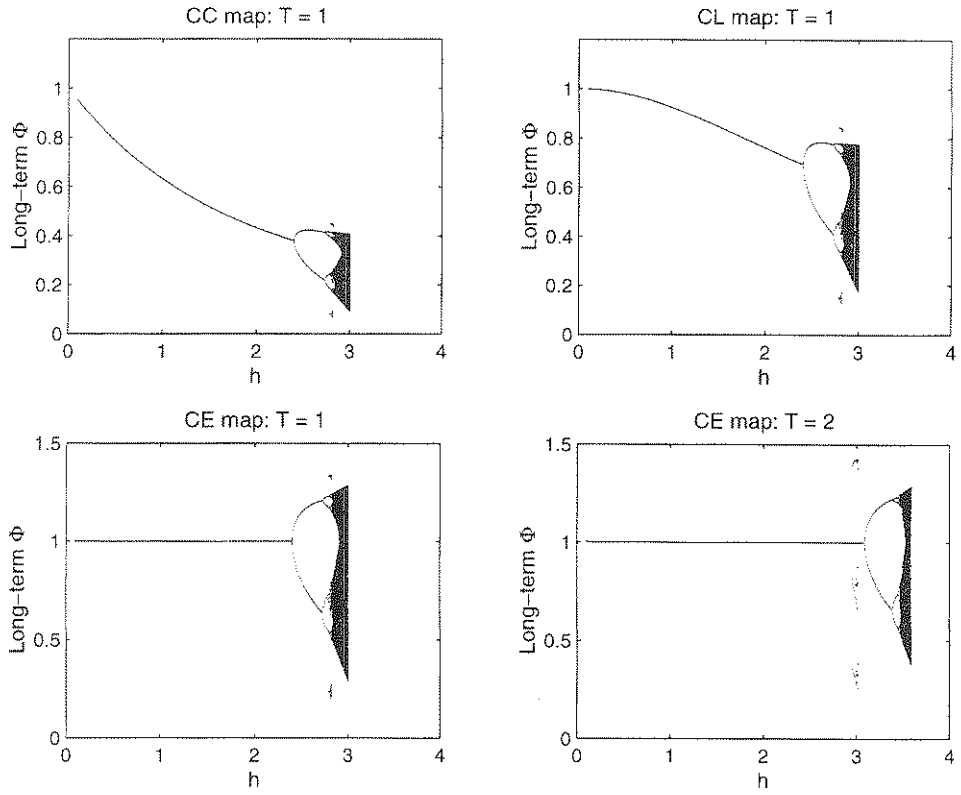

Fig. 3. Bifurcation diagram for the finite CC, CL and CE maps. See text for details.

appear to be stable low period orbits in the CE, LL and LE maps for h *below* the linearized stability limit. In the following sections we examine the existence and stability of period-2 and -3 solutions of the corresponding infinite maps.

5. Spurious period-2 solutions

The bifurcation diagrams indicate that the fixed point of some of the finite maps loses stability to period-2 solutions of (4.1). We now investigate this for the infinite map (2.2) by looking at existence and stability of period-2 solutions.

Period-2 solutions have the form

$$\Phi_n = \begin{cases} u & \text{for } n \text{ even}, \\ v & \text{for } n \text{ odd}, \end{cases} \tag{5.1}$$

with $u \neq v$. Substituting this into (2.2) yields

$$\left.\begin{aligned} v &= u + uh\,(1 - u\Sigma_0 - v\Sigma_1) \\ u &= v + vh\,(1 - v\Sigma_0 - u\Sigma_1) \end{aligned}\right\} \tag{5.2}$$

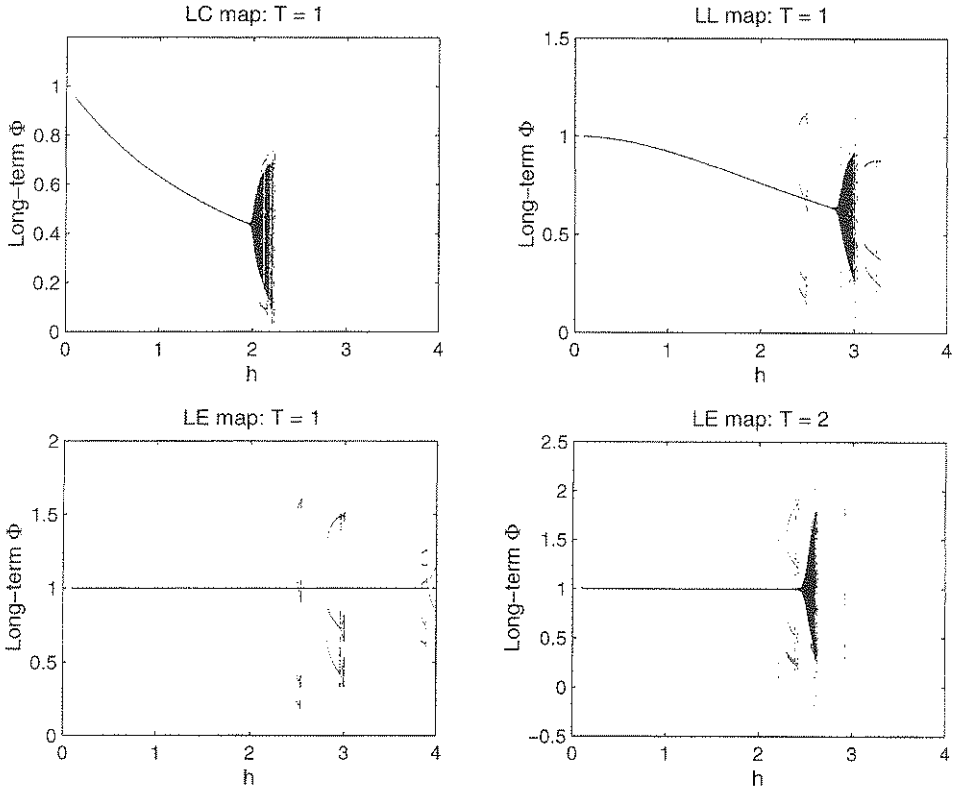

Fig. 4. Bifurcation diagram for the finite LC, LL and LE maps. See text for details.

where the even and odd sums Σ_0 and Σ_1 are defined by

$$\Sigma_\alpha = \sum_{l=0}^{\infty} \omega_{2l+\alpha} \quad \text{for } \alpha \in \{0,\ 1\}.$$

Eliminating v from (5.2) gives the quartic polynomial in u:

$$uh\left[u(\Sigma_0+\Sigma_1)-1\right]\left[u^2h^2\Sigma_0(\Sigma_0-\Sigma_1)-uh(h+2)(\Sigma_0-\Sigma_1)+h+2\right]=0. \tag{5.3}$$

Note that two solutions are the fixed points 0 and Φ^* of the map (2.2) whilst the period-2 solutions are the roots of the quadratic factor. The discriminant of the quadratic factor must be positive for real period-2 solutions to exist, i.e.,

$$h^2(h+2)(\Sigma_0-\Sigma_1)\big(h(\Sigma_0-\Sigma_1)-2(\Sigma_0+\Sigma_1)\big)>0. \tag{5.4}$$

The even and odd sums for the CC map are

$$\Sigma_0 = \frac{r}{(1-q)(1+q)}, \qquad \Sigma_1 = \frac{rq}{(1-q)(1+q)}$$

(recall that $r = h/T$ and $q = \mathrm{e}^{-r}$). Substituting into (5.4) gives the condition for real period-2 solutions as

$$h(1-q)-2(1+q)>0,$$

and this is also the condition for the CL and CE cases. Comparing this with the stability inequality (3.6) shows that period-2 solutions exist beyond the linear stability limit for these maps.

The odd and even sums for the LC map reduce to

$$\Sigma_0 = \Sigma_1 = \frac{r}{2(1-q)}$$

and so it follows from (5.4) that period-2 solutions do not occur for any h. Note that the stability equation for this case at $h = h^*$ is $z^2 - 2qz + 1 = 0$ and the roots are complex. Hence it is likely that the fixed point experiences a Hopf bifurcation at the stability limit (see Fig. 4).

The condition for period-2 solutions of the LL map is $h > 6(1+q)^2/(1-q)^2$. This is not satisfied as an equality when $h = h^*$ and so the fixed point Φ^* of this map does not bifurcate into period-2 solutions at the stability limit h^*.

Bifurcation into period-2 behaviour is only possible for the LE map when the first condition of (3.12) is the more restrictive, i.e., for $T < \approx 1 \cdot 10173$, and the difference in behaviour is illustrated in Fig. 4 which shows the long-term behaviour of the finite LE map when $T = 1$ and $T = 2$. There appears to be a period-2 bifurcation when $T = 1$ at $h^* \approx 3 \cdot 9$, and the figure also shows a range of other periodic solutions below the stability limit.

Finally, we note that there are no period-2 solutions for values of h below the linearized stability limit h^* for any of the six maps. (This follows immediately from comparing the Schur conditions for linear stability of Φ^* given in Section 3.1 with (5.4).)

5.1. Period-2 stability

We now show how the stability of period-2 solutions of (2.2) can be analyzed. The first step is to decide whether to perturb the period-2 solution for all n or just for $n \geqslant 0$. Since $\{\Phi_n\}$, $n < 0$, may be regarded as initial data, it makes sense just to perturb for $n \geqslant 0$ (this also simplifies the calculations). We linearize about the period-2 solution (u, v) from (5.2), setting $\Phi_{2m} \equiv u$ and $\Phi_{2m+1} \equiv v$ for $m < 0$, and write $\Phi_{2m} = u + \delta_m$, $\Phi_{2m+1} = v + \varepsilon_m$ for $m \geqslant 0$. After some rearrangement this gives the linear system

$$\left.\begin{aligned} \delta_m &= b_2\,\varepsilon_{m-1} - hv\sum_{k=1}^{m}[\omega_{2k-1}\,\delta_{m-k} + \omega_{2k-2}\,\varepsilon_{m-k}] \\ \varepsilon_m &= b_1\,\delta_m - hu\sum_{k=1}^{m}[\omega_{2k-1}\,\varepsilon_{m-k} + \omega_{2k}\,\delta_{m-k}] \end{aligned}\right\} \quad \text{for } m > 0$$

for the perturbations $(\delta_m, \varepsilon_m)$, where $b_1 = vu^{-1} - hu\omega_0$ and $b_2 = uv^{-1}$.

Setting $\underline{z}_m = (\delta_m, \varepsilon_m)^{\mathrm{T}}$ allows the linear system to be written as

$$\Gamma_0\,\underline{z}_m = \sum_{j=1}^{m}\Gamma_j\,\underline{z}_{m-j}, \tag{5.5}$$

in terms of matrices $\Gamma_j \in \mathbb{R}^{2\times 2}$ which depend on the particular map under consideration. For example, the CC map has

$$\Gamma_0 = \begin{pmatrix} -1 & 0 \\ b_1 & -1 \end{pmatrix}, \qquad \Gamma_1 = \begin{pmatrix} hvrq & hvr - b_2 \\ hurq^2 & hurq \end{pmatrix}, \qquad \Gamma_j = hrq^{2j}\begin{pmatrix} vq^{-1} & vq^{-2} \\ u & uq^{-1} \end{pmatrix}, \quad j \geqslant 2.$$

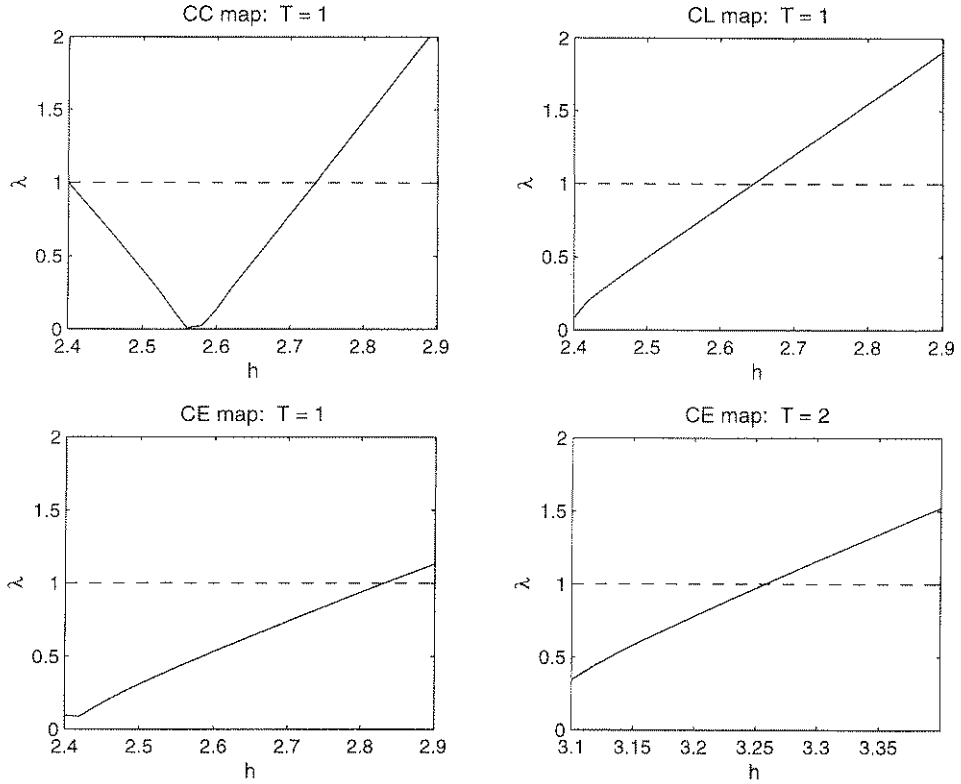

Fig. 5. Graph of the stability coefficient λ against time-step h for the CC, CL and CE maps. See text for details.

Eq. (5.5) can be written as

$$\underline{z}_m = P_m \underline{z}_0, \tag{5.6}$$

where the matrices $P_m \in \mathbb{R}^{2\times 2}$ are defined recursively in terms of the Γ_j by

$$P_0 = I, \qquad P_m = \Gamma_0^{-1} \sum_{j=1}^{m} \Gamma_j P_{m-j}, \quad m \geqslant 1. \tag{5.7}$$

It follows from (5.6) that the period-2 solution will be linearly stable to perturbations of this type (in the sense that $\|\underline{z}_m\|_2/\|\underline{z}_0\|_2$ is bounded for all $m > 0$) if the matrix 2-norm of the matrices P_m remains bounded as $m \to \infty$. It can be verified numerically that for large m ($m \geqslant 10$ is big enough) $\|P_m\|_2 \propto \lambda^m$ (where $\lambda > 0$ depends on the map under consideration, T and h). Hence the period-2 solution is stable provided $\lambda < 1$. Graphs of λ against h for the CE, CC and CL maps are shown in Fig. 5. The quantity λ is computed as the ratio $\|P_m\|_2/\|P_{m-1}\|_2$ for $m = 50$. There is good agreement between the time-step range for which the solutions are predicted to be stable by this analysis (i.e, for which $\lambda < 1$), and for which period-2 solutions are observed for the finite maps in Fig. 3.

Fig. 4 shows the fixed point of the finite LE map with $T = 1$ losing stability to a period-2 solution at $h \approx 3.9$. The linear perturbation matrices P_m for this map are bounded for h between $h^* = 3.9224$ and about 4.365, and the first plot of Fig. 6 shows a graph of $\|P_m\|_2$ against m at $h = 3.93$. The period-2

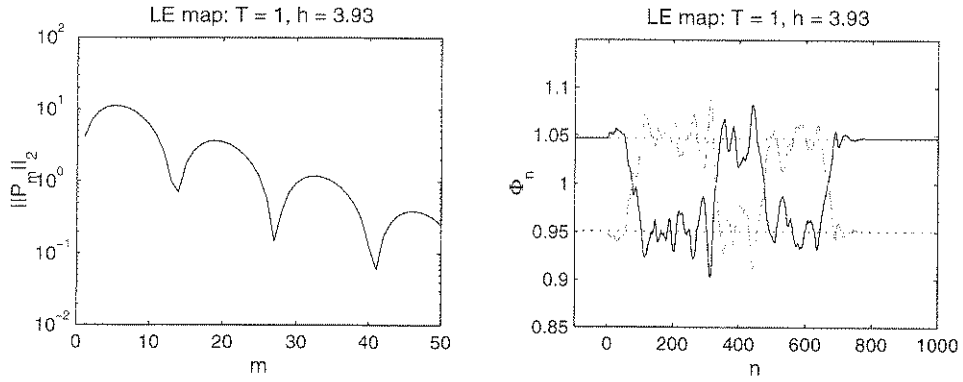

Fig. 6. Graph of $\|P_m\|_2$ for the LE map (left plot). The black (grey) curves in the right-hand plot show the solution Φ_n of the perturbed map when n is odd (even). The dotted lines are the period-2 solutions $u < v$.

solution appears to be very stable to random perturbations, as illustrated in the second plot of Fig. 6. Here the solution of the finite LE map is computed with $N = 100$ and with the initial condition that $\Phi_{-98} = \Phi_{-96} = \cdots = \Phi_{-2} = u$ and $\Phi_{-99} = \Phi_{-97} = \cdots = \Phi_{-1} = v$, where (u, v) is the period-2 solution and $u < v$. The iterates Φ_n for $n = 1, \ldots, 700$ are computed using a perturbed version of (4.1) formed by setting $\Phi_{n+1} = \Phi_{n+1} + \varepsilon_{n+1}$ at each stage, where the perturbations ε_n are chosen randomly to satisfy $|\varepsilon_n| < 1.5 \times 10^{-3}$ for all n. The final 300 iterates are computed from the (unperturbed) map (4.1). The solution wanders around close to one of the two levels of the period-2 solution and returns to it once the perturbations are switched off. If smaller perturbations are used then the solution remains close to the two values u and v for all n.

6. Spurious period-3 solutions

Many of the finite maps appear to have period-3 solutions in Figs. 3 and 4, with period-3 solutions seeming to exist below the linear stability limit in the CE and LE cases. We now investigate the existence and stability of period-3 solutions for the infinite maps.

Period-3 solutions satisfy

$$\Phi_n = \begin{cases} u & \text{if } n = 3l, \\ v & \text{if } n = 3l + 1, \\ w & \text{if } n = 3l + 2. \end{cases} \tag{6.1}$$

Substituting this into the general infinite map (2.2) yields the equations

$$v = u + uh(1 - u\Sigma_0 - w\Sigma_1 - v\Sigma_2), \tag{6.2}$$

$$w = v + vh(1 - v\Sigma_0 - u\Sigma_1 - w\Sigma_2), \tag{6.3}$$

$$u = w + wh(1 - w\Sigma_0 - v\Sigma_1 - u\Sigma_2), \tag{6.4}$$

where now the sums are given by

$$\Sigma_\alpha = \sum_{l=0}^{\infty} \omega_{3l+\alpha}, \quad \alpha \in \{0, 1, 2\}.$$

Eqs. (6.2)–(6.4) can be solved for u to yield

$$u\big[u(\Sigma_0+\Sigma_1+\Sigma_2)-1\big]F(u,h,\Sigma_0,\Sigma_1,\Sigma_2)=0, \tag{6.5}$$

where $F(u,h,\Sigma_0,\Sigma_1,\Sigma_2)$ is a sixth order polynomial in u with real coefficients (again the two linear factors correspond to the fixed points 0 and Φ^* of (2.2)). Reducing the equations to this form is complicated and was done using the symbolic manipulation package `Maple`. Our approach is to obtain w in terms of u and v from (6.2), and then substitute for w in (6.3) and (6.4) to obtain a pair of quadratic equations in v whose coefficients are functions of u. Eliminating the terms in v^2 then results in a linear equation for v in terms of u, and substituting for v in either of the quadratics and simplifying results in (6.5). For general T and h the roots of F are complex, and the coefficient terms in F are too complicated to enable us to find conditions on h that will guarantee that the period-3 solutions are real and positive. Such conditions can be found however in the case where the period-3 solutions are repeated roots of F, i.e., they correspond to the roots of the cubic polynomial $p(u)$ satisfying $F=p^2$. We now state conditions for this case to arise in general.

Consider the general sixth-order polynomial with real coefficients

$$q(x)=x^6+g_5x^5+g_4x^4+g_3x^3+g_2x^2+g_1x+g_0.$$

This will have three solutions of multiplicity two if it can be written as a cubic squared, i.e., if $q(x)=(x^3+ax^2+bx+c)^2$ for real a, b and c. Equivalently, the following conditions must be satisfied:

$$\begin{aligned} &g_0=c^2, && g_1=2bc, && g_2=2ac+b^2,\\ &g_3=2ab+2c, && g_4=a^2+2b, && g_5=2a. \end{aligned}$$

This gives the real coefficients in the cubic as

$$a=\tfrac{1}{2}g_5, \qquad b=\tfrac{1}{8}(4g_4-g_5^2), \qquad c=\tfrac{1}{16}(8g_3-4g_4g_5+g_5^3),$$

and the additional conditions

$$\left.\begin{aligned} 0 &= \tfrac{1}{256}(8g_3-4g_4g_5+g_5^3)^2-g_0\\ 0 &= \tfrac{1}{64}(4g_4-g_5^2)(8g_3-4g_4g_5+g_5^3)-g_1\\ 0 &= \tfrac{1}{16}g_5(8g_3-4g_4g_5+g_5^3)+\tfrac{1}{64}(4g_4-g_5^2)^2-g_2 \end{aligned}\right\} \tag{6.6}$$

must also be satisfied.

The roots of the cubic $p(x)\equiv x^3+ax^2+bx+c$ can be found by making the coordinate transformation $x=t-\frac{1}{3}a$, to give $t^3+Pt+Q=0$. The roots of this transformed cubic can be characterized by considering the quantity $D=(\frac{1}{3}P)^3+(\frac{1}{2}Q)^2$. We have $a=\frac{1}{2}g_5$, $b=\frac{1}{2}g_4-\frac{1}{2}a^2$ and $c=\frac{1}{2}g_3-ab$ giving

$$D=\tfrac{1}{13824}(25g_5^6-180g_5^4g_4+320g_5^3g_3+304g_5^2g_4^2-1152g_5g_4g_3+64g_4^3+864g_3^2). \tag{6.7}$$

The cubic has real roots when $D\leqslant 0$. If this condition is satisfied then the roots are positive provided the coefficients satisfy $a<0$, $b>0$ and $c<0$.

We have derived the general conditions for a 6th-order polynomial to have repeated real positive roots, and we now look at the roots of the polynomial F for the six different infinite maps. The infinite sums

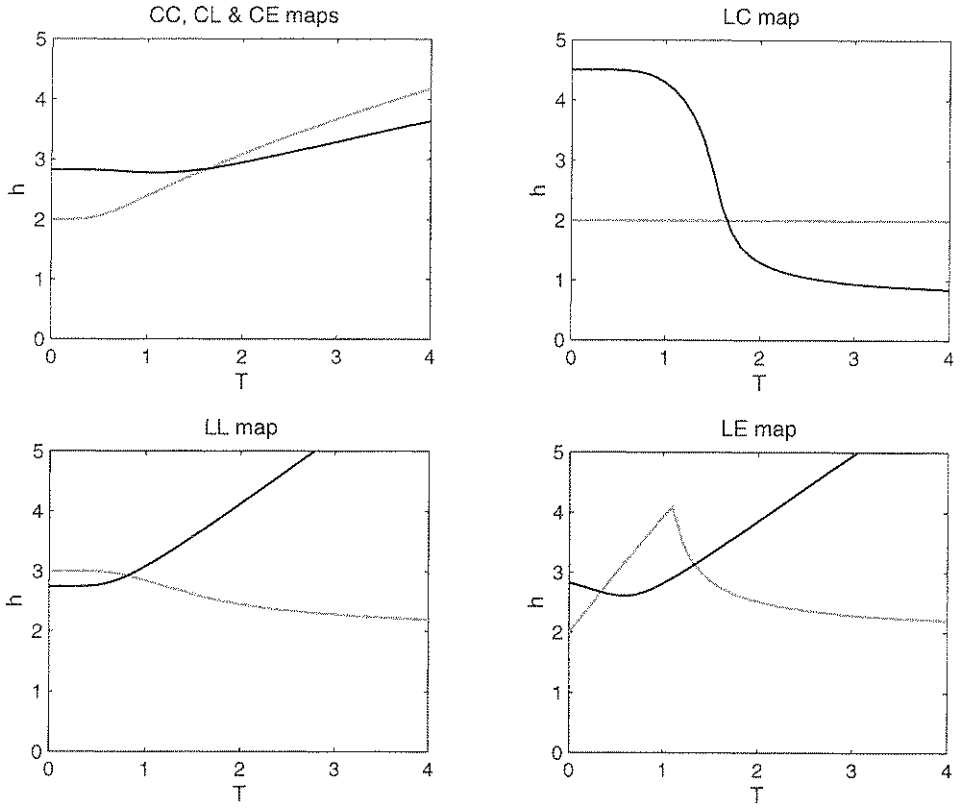

Fig. 7. Graphs of time-step h for which there are repeated period-3 solutions for each map (black line). The linear stability limit h^* of the fixed point is shown in grey for comparison.

for the CC case are $\Sigma_1 = q\Sigma_0$ and $\Sigma_2 = q^2\Sigma_0$ where $\Sigma_0 = r(1-q^3)^{-1}$, and in this case the three terms in (6.6) have the polynomial

$$Q_C(T,h) \equiv q^4(h+1)^2 - 4q^3 - 2q^2(h^2+3h+6) + 4q(h-1) + h^2 - 8$$

as highest common factor (hcf). This is also the hcf of these terms in the CL and CE cases. Hence there will be a repeated period-3 solution of these maps if and only if $Q_C(T,h) = 0$.

The hcf of the three terms in (6.6) for the LC, LL and LE maps are again polynomials in q whose coefficients are functions of h and $r = h/T$. In the LC case the hcf is a cubic, and the hcfs for the LL and LE maps are both (different) eighth order polynomials in q. In each case repeated period-3 solutions are only possible for values of h that make the hcf equal to zero for a given delay T. Graphs of time-step values for which there are repeated period-3 solutions for each of the maps are shown in Fig. 7. Note that for each map there are values of T for which these period-3 solutions exist below the linear stability limit h^*. We have checked the signs of D and the coefficients a, b, and c at each value of T and h shown, and in all cases the repeated period-3 solutions are real and positive.

If h is chosen to be slightly smaller than the time-step value for which there are repeated period-3 solutions then we found that F has six complex roots (in all the cases we looked at), and so there are no real period-3 solutions. Similarly, if h is chosen to be slightly larger than the time-step value for which

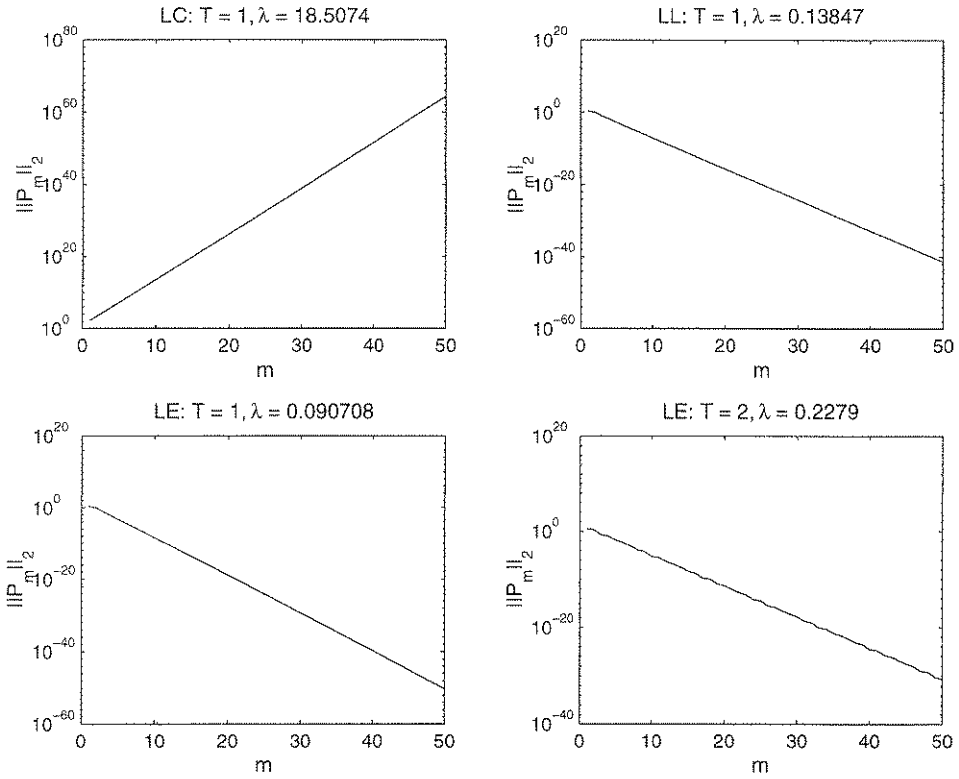

Fig. 8. Graphs showing $\|P_m\|_2$ against m for the repeated period-3 solutions of the LC, LL and LE maps for the values of T as labeled. The growth/decay rate λ for each of these maps is given in the title.

there are repeated period-3 solutions then F always appears to have six real positive roots, corresponding to two different period-3 solutions. The repeated solutions mark the transition between complex and real roots.

Note that the period-3 solutions of the finite maps shown in Figs. 3 and 4 are first seen for values of the time-step shown above to correspond to repeated period-3 solutions, and we now investigate their stability.

6.1. Period-3 stability

The stability of period-3 solutions can be analyzed in the same way as the period-2 solutions in Section 5.1. Perturbing the solution by setting $\Phi_{3m} = u + \delta_m$, $\Phi_{3m+1} = v + \varepsilon_m$, and $\Phi_{3m+2} = w + \gamma_m$ for $m \geqslant 0$ (where the period-3 solution is (u, v, w) given by (6.1)) and linearizing leads to an equation like (5.5), except that now the perturbation vectors and matrices are $\underline{z}_m = (\delta_m, \varepsilon_m, \gamma_m)^{\mathrm{T}} \in \mathbb{R}^3$ and $\Gamma_j \in \mathbb{R}^{3\times 3}$. This can be written more simply as

$$\underline{z}_m = P_m \underline{z}_0,$$

where the matrices $P_m \in \mathbb{R}^{3\times 3}$ are defined recursively in terms of the Γ_j by (5.7). Hence a period-3 solution will be stable if $\|P_m\|_2$ remains bounded as $m \to \infty$.

To compute the matrices P_m for the repeated period-3 solutions (at fixed T) we first calculate (using `Maple`) the time-step h for which they exist as shown in Fig. 7, and the coefficients a, b, and c of the cubic $p(x)$. From this the three (real and positive) repeated period-3 roots can be computed and without loss of generality we set u to be the minimum root. It is important to note that the ordering of the other two roots does matter, since in general if $u \to v \to w$ is a period-3 solution, then $u \to w \to v$ is not. In all cases we have found the period-3 solution to be $u \to v \to w$ with $u < v < w$. The matrices Γ_j can then be found by straightforward substitution, and the P_m computed from them using (5.7).

The linear stability matrices P_m for the repeated period-3 solutions are the same for the CC, CL and CE maps at a fixed value of T, and their norms are found to decay like λ^m for $\lambda = 0.60694$ when $T = 1$ and $\lambda = 0.20969$ when $T = 2$. The matrices P_m for the LC, LL and LE maps at the repeated period-3 solutions are all different. Graphs of $\|P_m\|_2$ against m for the maps and values of T corresponding to the bifurcation plots of Fig. 4 are shown in Fig. 8. The corresponding time-step values can be found from Fig. 7. The computed growth/decay rates λ are given in the title of each plot.

7. An adaptive algorithm

So far we have studied fixed time-step discretizations of the IDE (1.1). In this section we look at a variable time-step algorithm that is obtained by imposing a local error-control policy.

Following the standard practice for ODEs (see, for example, [5]) we set up an embedded pair of time-stepping formulas. This is done by combining the main formula (Euler) with a second-order formula (Improved Euler). A similar process has been examined in [7] for a delay differential equation.

The algorithm can be written in terms of the following quantities:

$$k_1 := \Phi_n\left(1 - \sum_{j=0}^{\infty} \Phi_{n-j}\omega_{j,n}\right), \tag{7.1}$$

$$\Phi_{n+1} := \Phi_n + h_n k_1, \tag{7.2}$$

$$k_2 := \Phi_{n+1}\left(1 - \sum_{j=0}^{\infty} \Phi_{n+1-j}\omega_{j,n+1}\right), \tag{7.3}$$

$$\mathrm{est}_{n+1} := \tfrac{1}{2}h_n|k_2 - k_1|, \tag{7.4}$$

$$h_{\mathrm{new}} := h_n\left(\frac{\theta\tau}{\mathrm{est}_{n+1}}\right)^{1/2}, \tag{7.5}$$

where the weights $\{\omega_{j,n}\}$ now depend upon n and satisfy

$$\omega_{j,n} \approx \int_{t_{n-j-1}}^{t_{n-j}} K(t_n - s)\,\mathrm{d}s. \tag{7.6}$$

Note that the time-step $h_n := t_{n+1} - t_n$ may now vary with n. The quantities k_1 and k_2 represent stage-values for the two ODE formulae, est_{n+1} is the local error estimate for the step, τ is a user-supplied error tolerance, $\theta \in (0, 1)$ is a safety factor and h_{new} is the next time-step to be used. (When the time-step is constant the formula for Φ_{n+1} reduces to (2.2).)

The overall algorithm for a single step from t_n to $t_n + h_n$ may now be written as

(1) Compute k_1, Φ_{n+1}, k_2, est_{n+1} and h_{new}.

(2a) If $\text{est}_{n+1} > \tau$ then reject the step. Set $h_n = h_{\text{new}}$ and return to (1).

(2b) Otherwise ($\text{est}_{n+1} \leqslant \tau$) accept the step. Set $h_{n+1} = h_{\text{new}}$.

Here we are concerned with the long-term behaviour of numerical methods for (1.1). The variable time-stepping algorithm is more complicated than the fixed-step discretizations analyzed in earlier sections; however, by making appropriate assumptions it is possible to obtain some insights.

We have seen that the fixed time-step discretization permits spurious solutions. It is generally accepted that conventional error-control algorithms are successful at suppressing such spurious behaviour and a rigorous justification of this, for the case of ODEs, is given in [2]. Hence it is reasonable to assume that the above algorithm computes a solution that is close to the correct steady state of $\phi(t) \equiv 1$. We will therefore linearize perturbations about this solution and consider the problem

$$\frac{\mathrm{d}}{\mathrm{d}t}\phi(t) = -\int_{-\infty}^{t} \phi(t)K(t-s)\,\mathrm{d}s \tag{7.7}$$

for the kernel (1.3).

The basic aim of the adaptive algorithm is to take the largest possible time-step, subject to the local accuracy requirement. Hence, once the numerical solution has approached the steady state we would expect the algorithm to choose time-steps that are roughly at the boundary of the interval of stability. This type of behaviour has been studied by Hall [6] and Higham and Famelis [8] for ODEs and delay differential equations, respectively. They showed that in certain circumstances, it is possible to define equilibrium states where the method computes solutions that are within $O(\tau)$ of the exact steady state and with a time-step that is exactly on the stability boundary. We show below that this analysis carries through to the Eq. (7.7).

First, we mention that it is important to perform the integration accurately in computing the weights (7.6). If we were to use simple quadrature rules based on piecewise constant or linear approximations of the kernel, then the steady state of the discrete method would not be a sufficiently accurate approximation of the true steady state (see, e.g., Fig. 1). In this case the error control criterion would require an extremely small time-step in order for the steady state to be resolved to within the tolerance. In other words, the time-step would always be limited by an accuracy requirement, rather than the stability constraint. Numerical experiments have confirmed this effect.

Henceforth, we assume that the weights in (7.6) correspond to the PC solution approximation and are computed by integrating the kernel exactly (i.e., we consider the linearized CE map). Our approach, based on insights from the delay-differential equation case [8] is to look for an equilibrium state of the linearized version of the adaptive recurrence (7.1)–(7.5) with a constant time-step, $h_n \equiv h$, and an oscillating solution $\phi_j = (-1)^j v$. Substituting this into (7.1) and (7.2) for the linearized problem gives

$$-v = v - hv\sum_{j=0}^{\infty}(-1)^j\,\omega_j$$

($\omega_{j,n} = \omega_j$ since the time-step h_n is constant), which we write as

$$-v = v - hv(\Sigma_0 - \Sigma_1), \tag{7.8}$$

where the even and odd sums Σ_0 and Σ_1 for the CE map are

$$\Sigma_0 = \frac{1}{1+q} \quad \text{and} \quad \Sigma_1 = \frac{q}{1+q}$$

(recall that $q = \mathrm{e}^{-r}$, $r = h/T$). Hence, in (7.8) we find the fixed time-step is given by

$$h = \frac{2(1+q)}{1-q}. \tag{7.9}$$

In order for a fixed time-step to be chosen by the algorithm, we require $\mathrm{est}_{n+1} = \theta\,\tau$ in (7.5). We have

$$|k_2 - k_1| = \left| \sum_{j=0}^{\infty} \omega_{j,n}(\Phi_{n-j} - \Phi_{n+1-j}) \right| = \left| \sum_{j=0}^{\infty} \omega_{j,n} 2v \right| = 2|v|,$$

so, using (7.4), this requirement reduces to

$$|v| = \frac{\theta\tau}{h}. \tag{7.10}$$

In summary, Eqs. (7.9) and (7.10) define a period-two equilibrium state of the numerical algorithm. Note that the time-step in (7.9) precisely corresponds to the boundary of stability (3.6) for the CE map. Hence, in this mode, the algorithm is taking the largest stable time-step. Also, note that (7.10) ensures that Φ_n is within $\mathrm{O}(\tau)$ of the correct steady state. In practice we would expect the algorithm to approach this equilibrium state. If the equilibrium is stable—in the sense that it is locally attractive as a solution to the discrete recurrence for $\{h_n, \Phi_n\}$—then it should be observed exactly. However, in the case of an unstable equilibrium we would expect the algorithm to exhibit small-scale fluctuations around these values. Typically, the error-control process takes h_n close to the value in (7.9), the instability with respect to small perturbations causes h_n to move away, and if h_n becomes too large the error-control criterion forces a reduction via a rejected step.

To illustrate the relevance of the equilibrium state, we present results for the adaptive algorithm applied to (1.1) with kernel (1.3) and $T = 1$ with the initial condition $\phi(t) = 0$ for $t < -10$ and $\phi(t) = 2$ for $-10 \leqslant t \leqslant 0$. We chose a tolerance of $\tau = 10^{-3}$ and a safety factor of $\theta = 0 \cdot 8$. The problem was solved for $0 < t \leqslant 500$, and we present results for the last 100 steps, which typify the long-term behaviour. The upper plot in Fig. 9 shows the departure of the numerical solution from the steady state $\phi(t) \equiv 1$, measured as $\gamma_n := (\Phi_n - 1)/\theta\tau$. For the equilibrium state defined by (7.9) and (7.10), γ_n alternates between $\pm 1/h^*$, where $h^* \approx 2 \cdot 399$ is the time-step at the stability limit—these values are marked with dashed lines on the plot. It is clear that the numerical solution is approximately following the quantities defined by (7.9) and (7.10). The lower plot in Fig. 9 gives the time-steps, and it can be seen that the values oscillate around h^* (marked by a dashed line). Overall, the behaviour is consistent with an unstable equilibrium of the map that takes $\{h_n, \Phi_n\}$ to $\{h_{n+1}, \Phi_{n+1}\}$; see, for example, the results reported in [6]. Approximately one in four steps is rejected and the numerical solution oscillates about the equilibrium values.

8. Summary

Our overall aim in this work is to study the behaviour of a discrete version of a nonlinear integro-differential equation. As in the recent references [1,2,4,7,9], our results are derived from a numerical

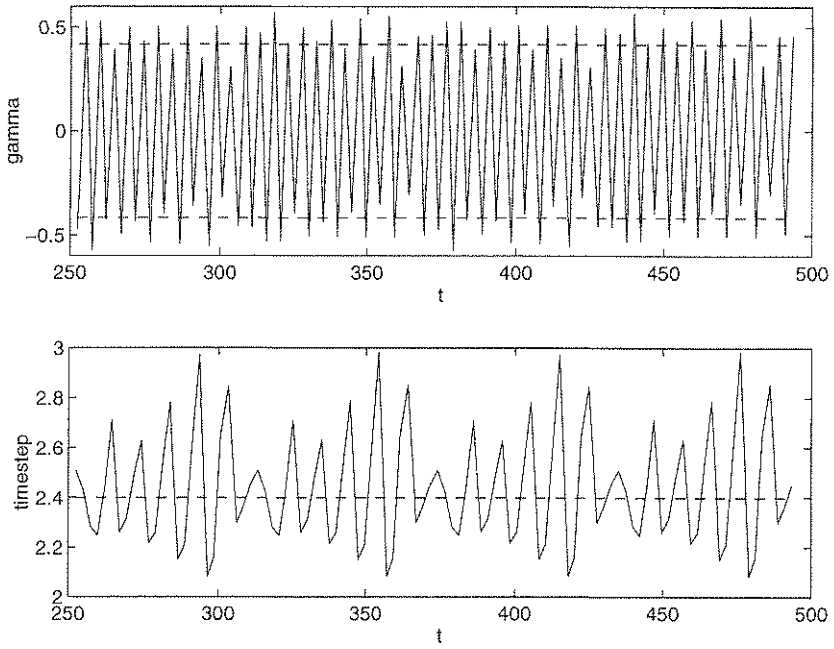

Fig. 9. Long time behaviour of the adaptive algorithm (see text for details).

analysis perspective with emphasis on spurious behaviour that arises below, or near, the linear stability limit of the true fixed point. We believe this to be the first systematic study of the occurrence and stability of low period spurious solutions for a nonlinear integro-differential model. The map produced is infinite, in the sense that the approximation at t_n depends on *all* earlier approximations. To specify a complete algorithm requires choices to be made about

- the basic quadrature method,
- the accuracy with which the kernel is integrated, and
- the treatment of the infinite tail.

The zero fixed point of the underlying continuous problem (1.1), (1.3) is unstable. For each of the numerical methods considered here the corresponding zero fixed point is also unstable for all $h > 0$. The time-step h^* at which the non-zero fixed point loses stability is plotted as a function of the delay parameter T in Fig. 2. (Recall that the non-zero fixed point $\phi(t) \equiv 1$ for the underlying continuous problem (1.1), (1.3) is stable for all $T > 0$.) We also note the following key points.

- In the limit $T \to \infty$, the CC, CL and CE maps have a time-step restriction that is unbounded, whereas the LC, LL and LE maps require $h \leqslant 2$.
- Previous studies on hereditary influences have produced examples where introducing a small delay improves the stability (see, for example, [12]). From Fig. 2 we see that this behaviour also arises for the CC, CL, CE and LE maps, but the converse happens in the LL case.
- The type of bifurcation at the stability boundary varies with the choice of quadrature and kernel approximation.

The bifurcation diagrams Figs. 3 and 4 indicate that behaviour with respect to spurious low period solutions depends strongly on the precise details of the discretization. We have therefore investigated

period-2 and -3 solutions, showing that in some cases period-2 solutions can be ruled out, and in others they exist only beyond the linear stability limit h^*. We have developed a technique for studying the stability of these period-2 solutions which involves the unusual recurrence (5.6), and the stability analysis gives results that agree with the bifurcation diagrams. We have also been able to characterize a class of period-3 solutions that are observable in practice. A stability analysis confirms the existence of stable, positive period-3 solutions below the linear stability limit.

It is generally accepted that including an adaptive error control and time-step selection component serves to eliminate spurious behaviour. Tests with the the variable time-step algorithm in Section 7 are in agreement with this belief. Furthermore, insight into the performance of the algorithm can be found by linearizing about the true fixed point, defining an equilibrium state, and studying its stability. Here the concept of 'stability' relates to the local behaviour of the process around the correct fixed point—the instability in the process leads to inefficiency (via rejected steps) rather than inaccuracy. Overall, the adaptive process performs successfully, and in accord with the equilibrium analysis.

References

[1] M.A. Aves, P.J. Davies, D.J. Higham, Fixed points and spurious modes of a nonlinear infinite-step map, in: D.F. Griffiths and G.A. Watson (Eds.), Numerical Analysis: A.R. Mitchell 75th Birthday Volume, World Scientific, 1996, pp. 21–38.

[2] M.A. Aves, D.F. Griffiths, D.J. Higham, Does error control suppress spuriosity? SIAM J. Numer. Anal. 34 (1997) 756–778.

[3] J.M. Cushing, Integrodifferential Equations and Delay Models in Population Dynamics, Lecture Notes in Biomathematics, Springer, Berlin, 1977.

[4] D.F. Griffiths, P.K. Sweby, H.C. Yee, On spurious asymptotic numerical solutions of explicit Runge–Kutta methods, IMA J. Numer. Anal. 12 (1992) 319–338.

[5] E. Hairer, S.P. Nørsett, G. Wanner, Solving Ordinary Differential Equations I, Nonstiff Problems, 2nd Edition, Springer, Berlin, 1993.

[6] G. Hall, Equilibrium states of Runge–Kutta schemes, ACM Trans. Math. Software 11 (1985) 289–301.

[7] D.J. Higham, The dynamics of a discretized nonlinear delay differential equation, in: D.F. Griffiths and G.A. Watson (Eds.), Numerical Analysis 1993: Proceedings of the 15th Dundee Conference, Pitman Research Notes in Mathematics, Vol. 303, Longman Scientific and Technical, 1994, pp. 167–179.

[8] D.J. Higham, I.Th. Famelis, Equilibrium states of adaptive algorithms for delay differential equations, J. Comput. Appl. Math. 58 (1995) 151–169.

[9] A. Iserles, Stability and dynamics of numerical methods for nonlinear ordinary differential equations, IMA J. Numer. Anal. 10 (1990) 1–30.

[10] J.D. Lambert, Numerical Methods for Ordinary Differential Systems: The Initial Value Problem, Wiley, New York, 1993.

[11] Ch. Lubich, On the stability of linear multistep methods for Volterra convolution equations, IMA J. Numer. Anal. 3 (1983) 439–465.

[12] R.M. May, Time-delay verses stability in population models with two and three trophic levels, Ecology 54 (1973) 315–325.

[13] R.M. May, Mathematical aspects of the dynamics of animal populations, in: S.A. Levin (Ed.), Studies in Mathematical Biology, Part II, MAA Studies in Mathematics, Vol. 16, Mathematical Association of America, 1978, pp. 317–366.